Environmental Science Advances

ROYAL SOCIETY OF CHEMISTRY

PAPER

View Article Online
View Journal | View Issue

Cite this: *Environ. Sci.: Adv.*, 2025, **4**, 1054

Chemodosimetric sensing of hydrazine *via* an irreversible reaction-based sensor and its multifunctional applications†

Jhorna Borah,[a] Arati Chetry,[a] Anisha Pegu,[a] Pankaj Dutta,[b] Anupaul Baruah *[a] and Prithiviraj Khakhlary *[a]

Received 12th September 2024
Accepted 5th March 2025

DOI: 10.1039/d4va00339j

rsc.li/esadvances

Herein, we developed a very easy-to-synthesize, cost-effective and efficient chemosensor for hydrazine using readily available starting materials. The probe exhibited high sensitivity and selectivity for hydrazine in the presence of other interfering analytes through an irreversible reaction-based mechanism. The changes in the photophysical properties of the chemosensor in presence of this analyte were visible to the naked eye. The limit of detection (LOD) of hydrazine was found to be 1.7 ppb, indicating that even trace amounts could be detected. For on-site sensing of the mentioned analyte, the probe was immobilized in a naturally abundant starch-PVA polymer matrix. Hydrazine induced a visual colour change in the resulting composite film, enabling its on-site detection. The practical application of the probe was also demonstrated, which showed that the probe can detect the analyte in water and soil samples. The mechanism of sensing was established *via* NMR titration. The photophysical properties of the chemosensor before and after treatment with hydrazine were validated with theoretical studies.

Environmental significance

Hydrazine is a highly toxic chemical and can contaminate water, soil and air owing to its high water solubility and volatility, leading to various adverse effects on the environment and mankind. However, it is still being used in many sectors, causing serious contamination in the environment upon leakage. Hence, it is categorized as a carcinogen by the U.S. EPA with a threshold limit value of 10 ppb. Therefore, it is highly important to develop sensors to detect even trace concentrations of this analyte. Herein, we report the development of a simple and cost-effective onsite sensor for detecting trace amounts of hydrazine in the solution and vapour phases. The detection of hydrazine using the sensor was successfully performed in real samples like water and soil.

1. Introduction

Amines are important organic compounds and they are considered to be active ingredients in biological metabolism. However, abnormally high level of amines serves as a biological marker for food spoilage as well as diseases such as lung cancer, hepatopathy and uremia.[1–5] One such amine is hydrazine, which has substantial applications in chemical, pharmaceutical and agricultural industries ranging from catalysis, corrosion inhibitors and textile industry to pesticides.[6–12] Hydrazine is a rocket fuel used in missiles and satellite propulsion systems because of its properties like high flammability and high combustion.[12–14] But the excessive use of this amine raises its concentration levels in water and soil.[3] Moreover, certain yeast and nitrogen-fixing bacteria produce hydrazine as a byproduct in various biochemical reactions occurring in nature.[14–16] Leakage of hydrazine, either during manufacture, transport, consumption or disposal, can lead to serious contamination in the environment.[17,18] Furthermore, as hydrazine is water soluble and volatile, it can severely contaminate water, soil and air in the environment. Moreover, the circulation of hydrazine-containing waste through the ecosystem has various adverse effects on the environment. It can inhibit seed germination, thereby obstructing plant growth, and it is also known to be responsible for the wilting of leaves.[19]

Owing to its volatile nature, it can easily enter the human and animal body either by inhalation or through oral or dermal exposure. Prolonged exposure to such amines leads to severe health issues such as dermal corrosion, mutagenesis of the liver, kidney and lungs, cancer and irreversible deterioration of the nervous system through skin absorption.[4,11,20] Because of these reasons, it is considered as a carcinogen by the US Environmental Agency, and thus, the threshold limit of hydrazine is set at 10 ppb in drinking water.[4,7,11,21,22] Therefore, selective and

[a]*Department of Chemistry, Dibrugarh University, Dibrugarh 786004, Assam, India. E-mail: pkhakhlary@dibru.ac.in*

[b]*Department of Physics, Dibrugarh University, Dibrugarh 786004, Assam, India*

† Electronic supplementary information (ESI) available. See DOI: https://doi.org/10.1039/d4va00339j

sensitive sensing of hydrazine in the gas as well as liquid phase using analytical methods has grabbed special attention.

Earlier, various methods, such as voltammetry, electrochemistry, surface-enhanced Raman spectroscopy and high-performance liquid chromatography (HPLC), were used for the estimation of hydrazine, but they were quite time-consuming, expensive and required tedious operational strategy.[23–26] Therefore, recently, colorimetric and/or fluorescent technology have emerged with superior properties, such as simplicity, low cost, easy operation, high sensitivity and selectivity, as well as *in situ* and *in vivo* monitoring performances.[26,27] Among these, reaction-based probes have grabbed significant attention because of their capability for site-specific reactions with various analytes, such as deprotection of esters in the presence of hydrazine and hydrazine-driven cleavage of cyanoethylene moieties.[28–31]

It is a well-known fact that the development of effective optical sensors for toxic ions occupies a broad area in supramolecular chemistry,[32,33] and there is no need to talk about the toxicity of cyanide in the environment. Cyanide can bind to the active site of cytochrome oxidase, inhibiting cellular respiration and eventually leading to death.[34–38] In spite of its severe toxicity, it has multiple uses in industrial fields, such as plastic manufacture and electroplating mining.[34,36–40] Cyanide is also found in many naturally occurring foods such as cassava, taro, and apple seeds.[40,41] Therefore, detection of cyanide in low concentration level is highly important. Among all the fluorescent detection techniques for ions, currently, the chemodosimeter approach has gained special importance because of its advantages over other approaches.[32,39] Herein, the interference from other ions is very less and the selectivity of sensing is high, which is quite opposite in case of other approach such as the acid base mechanism. Recently, the development of cyanide sensors based on nucleophilic addition reactions has gained importance because of its high nucleophilicity as compared to other anions. Such sensors are mainly based on the nucleophilic attack of CN^- to electrophilic double bonds such as C=C, C=O, C=N, C=S.[38,41–45]

Considering the above challenges, herein, we report a simple, cost-effective and very easy-to-synthesize chemosensor for hydrazine and cyanide starting from 9-anthraldehyde and malononitrile. The synthesized probe can discriminately detect both hydrazine and CN^- through two different mechanisms. In the case of hydrazine, the dicyanovinyl moiety is replaced, and a new compound is formed. Meanwhile, for the CN^- ion, the dicyanovinyl moiety acts as the binding site. The CN^- ion attacks the C=C double bond of the sensor through a nucleophilic addition reaction. The driving force of this reaction is the stabilization of the electron-withdrawing dicyanovinyl group through π-conjugation owing to the addition of cyanide. The sensing is also extended to real samples like water and soil in the case of hydrazine and water and food samples for CN^-, which establishes the practical applicability of the probe.

Some of the malononitrile-based sensors for the detection of hydrazine and CN^- are listed in Tables S1 and S2,† respectively, for comparison.

2. Experimental section

2.1. General methods

All the chemicals purchased were of analytical grade and used without further purification. 9-Anthraldehyde and malononitrile were purchased from Spectrochem Pvt. Ltd, and hydrazine hydrate was purchased from SRL Chemicals. The solvents used were of spectroscopic grade. UV-vis spectra were recorded on a Shimadzu UV-1700 PharmaSpec spectrophotometer with a quartz cuvette featuring a path length of 10 mm with a 2 mL solution against a solvent reference. Fluorescence spectra were recorded in a Horiba Jobin Yvon Fluoromax-4 Spectrofluorometer with a quartz cuvette of path length 1 cm. LC-MS (Liquid Chromatography-Mass Spectrometry) spectra were recorded in a Thermo Fischer Ultimate3000/TSQEndura spectrometer. ^{1}H-NMR and ^{13}C-NMR spectra were recorded on a Bruker 500 MHz and 126 MHz NMR spectrometer, respectively, applying tetramethylsilane as an internal standard. Chemical shifts are given in ppm.

2.2. Synthesis of probe 1

The probe was synthesized following a reported procedure with some modifications (Scheme 1).[1] 1 mmol of both 9-anthraldehyde and malononitrile were mixed with NaOH (1 mg) in H_2O : EtOH in the ratio 4 : 1 at 50 °C. At the end of the reaction, the precipitate was filtered off and dried. The crude product was purified by recrystallization (hexane:dichloromethane). The product was obtained as an orange powder (90% yield). LC-MS-$[M + 1]^+$ peak at $m/z = 255.11$. ^{1}H-NMR (500 MHz, $CDCl_3$): δ 8.95 (s, 1H), 8.66 (s, 1H), 8.11 (d, $J = 8.4$ Hz, 2H), 7.94 (d, $J = 8.8$ Hz, 2H), 7.69 (m, 2H), 7.60 (m, 2H). ^{13}C-NMR (126 MHz, $CDCl_3$): δ 160.47, 132.61, 130.81, 129.53, 129.11, 128.58, 126.09, 123.91, 123.39, 111.44, 113.13, 92.39.

2.3. Preparation of paper strips

For the paper strip test, strips were prepared from filter paper. First, the filter paper was cut into small, equal pieces in rectangular shapes. These strips of filter papers were then dipped into the probe solution in THF and allowed to dry. Then, the same strips were immersed in the solutions of different analytes prepared in THF and dried again.

2.4. Computational study

All computational calculations and analyses were performed using Avogadro,[46] ORCA 5_0_4,[47] and ChemCraft[48] software. The initial guess structures for both reactant and product were created and optimized in Avogadro. The ground state optimization for both reactant and product was performed using the Becke, 3-parameter, Lee–Yang–Parr (B3LYP) hybrid Generalized Gradient Approximation (GGA) functional with the def2-TZVP (valence triple-zeta polarization) basis set and D4 dispersion correction in ORCA 5_0_4 package. Optimizations are performed without any Resolution of Identity (RI) approximations. During optimization, vibrational frequency calculations were performed to confirm the convergence to the global minima. In

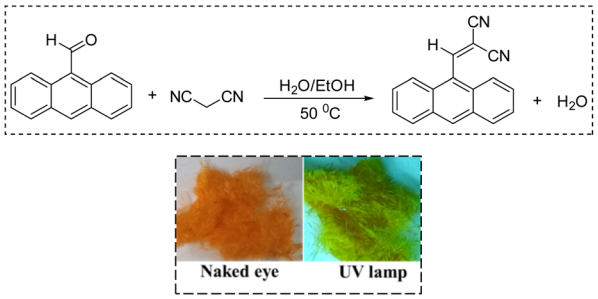

Scheme 1 Synthesis of the probe. (Inset) Solid-state images of the probe visualized with the naked eye and under a UV lamp.

all calculations, the Conductor-like Polarizable Continuum Model (CPCM) correction is done to incorporate the solvent effect of THF.

Utilizing the optimized ground state, the UV-visible spectra for both the reactant and product are obtained using the Similarity Transformed Equation of Motion Coupled Cluster Singles and Doubles (STEOM-CCSD) method, which includes correlation energy into the calculation of the excited state and thereby increases accuracy. This is done using the recently developed Domain-based Local Pair Natural Orbital (DLPNO) scheme, which decreases the computational cost while maintaining accuracy. During this calculation, the RIJCOSX approximation is used. The Resolution of Identity (RI) approximation is used for Coulomb integrals (J), while chain of sphere exchange (COSX) approximation is used for Hartree–Fock (HF) exchange integrals.

To obtain the fluorescence spectra, the excited state geometries of both reactant and product are optimized using Time-Dependent Density Functional Theory (TD-DFT) calculations. In this optimization step, the B3LYP/def2-TZVP level theory is applied with the D4 dispersion correction and CPCM correction for the solvent effect and without any RI approximation. ORCA_ESD module is used to calculate the excited state dynamics to predict the fluorescence spectra for both reactant and product.

3. Results and discussion

3.1. Design and synthesis of the probe

Hydrazine-mediated cleavage of the dicyanovinyl group is a well-established phenomenon. Considering this, a very easy-to-synthesize D–π–A probe was designed by connecting a donor (anthracene moiety) and an acceptor group (dicyanovinyl moiety). The olefinic bond is cleaved by the hydrazine moiety to produce a new compound, leading to a ratiometric change in the UV-vis spectra. In addition, there are literature studies that suggest the detection of cyanide by probes containing malononitrile moiety. Hence, we have also extended the sensing applications to cyanide. The olefinic bond that connects the donor and the acceptor can selectively accept CN^- ion owing to its high nucleophilicity over other anions. Thus, the conjugation of the system is interrupted by the addition of CN^- along with the ICT transition between the donor and the acceptor moiety. Thus, our synthesized probe can detect both the analytes through different mechanisms and thereby not interfere in the detection of each other.

3.2. Study of the sensing activity by the probe

The probe was synthesized and characterized by LC-MS, ^{1}H-NMR and ^{13}C-NMR spectroscopy. The spectral properties of the probe were examined with different neutral analytes *viz.* hydrazine hydrate, triethylamine (TEA), diisopropyl ethyl amine (DIPEA), *N*,*N*-diisopropyl amine (DIPA), ammonia, urea, thiourea as well as anions *viz.* F^-, Cl^-, Br^-, I^-, CN^-, AcO^-, N_3^-, SCN^-, S^{2-} by UV-vis and fluorescence spectroscopy. All the anions were taken as tetrabutyl ammonium salts (except S^{2-} which is taken as Na_2S) and all solutions, *i.e.*, the host and guest species, were prepared in THF in 10^{-5} M and 10^{-4} M concentrations, respectively. The solution of the probe is yellow in colour and absorbs at 428 nm wavelength. On addition of NH_2NH_2 and TBACN solution, it shows different changes in the absorption as well as emission spectra, which indicates different sensing mechanisms for the guest and host.

3.3. Absorbance study towards different amines by the probe

The probe was taken at 10^{-5} M concentration, and the absorbance was recorded. On adding an aliquot amount of hydrazine solution in THF (10^{-4} M), the absorbance of the peak at 428 nm decreased and finally diminished with the formation of a new peak at 390 nm (Fig. 1a and b). Consequently, the colour of the solution also changed from yellow to light green, enabling naked-eye detection of the sensing process. The simultaneous decrease and increase of the peak at 428 nm and 390 nm, respectively, give rise to a ratiometric change in the absorption spectra, indicating the formation of a new species. The saturation is obtained upon the addition of approximately 1 equiv. of hydrazine.

The absorbance *vs.* concentration plot displays a straight line with a high regression coefficient of ($R^2 = 0.98$) (Fig. S4a†). The LOD is calculated and found to be 1.7 ppb, which is much below the threshold limit value (10 ppb) as recommended by the US Environmental Protection Agency (EPA). Also, the binding constant calculated using the Benesi–Hildebrand equation is 1.25×10^4 M^{-1} (Fig. S4b†).

Based on these changes in the absorption spectra, a new compound is assumed to be formed between the probe and hydrazine. The plausible mechanism is given in Scheme 2.

No changes were observed in the absorption spectra of the probe in the presence of other aforementioned amines, even after the addition of an excess amount (Fig. S5†).

3.4. Selective sensing of the probe towards NH_2NH_2 over other neutral analytes

To identify possible interferences from other neutral species, UV-vis spectra were recorded for the probe with hydrazine in the presence of other common amines, *viz.*, TEA, DIPEA, DIPA, ammonia, urea and thiourea. It was found that there is no interference in the sensing process of hydrazine (Fig. 2), even in the presence of excess amounts of other amines. The selectivity

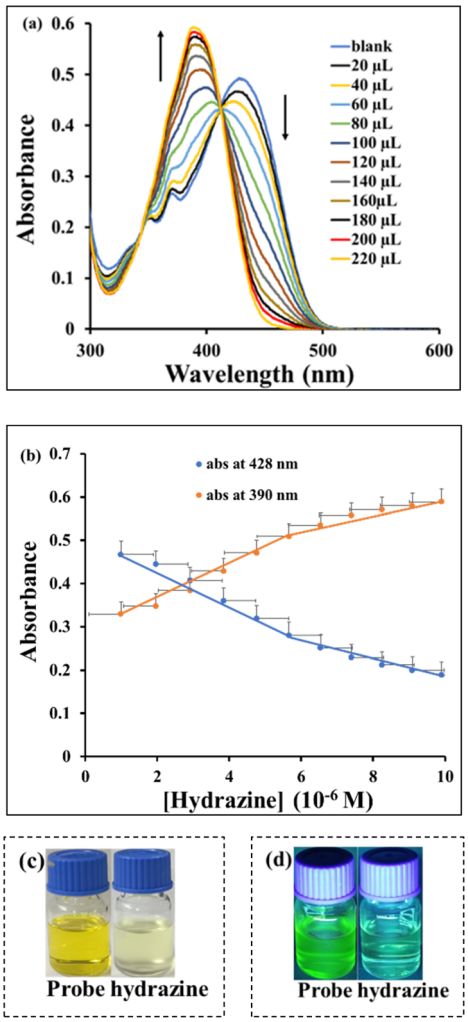

Fig. 1 (a) Overlaid absorption spectra of probe 1 (10^{-5} M) with hydrazine (10^{-4} M) in THF, (b) absorbance at 390 nm and 428 nm with increasing concentration of hydrazine. Colour changes of the probe with hydrazine visible with (c) naked eye and (d) under a UV lamp.

of the probe towards hydrazine over other analytes could be mainly attributed to the α effect of hydrazine, which makes it comparatively more reactive than other common amines.

3.5. Fluorescence sensing of hydrazine by the probe

The probe solution in THF (10^{-3} M) exhibits an emission peak at 504 nm upon excitation at a wavelength of 368 nm. There is an internal charge transfer (ICT) transition in the probe from the donor anthracene moiety to the electron-deficient

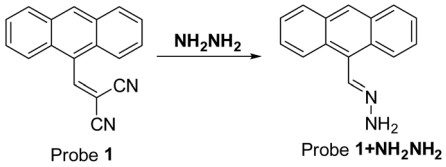

Scheme 2 Plausible reaction mechanism between hydrazine and probe 1.

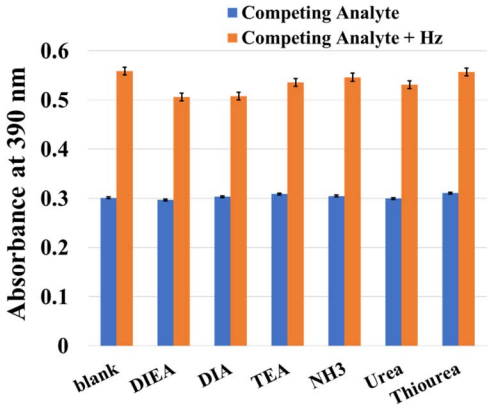

Fig. 2 Interference studies of probe 1 (10^{-5} M) with hydrazine (10^{-4} M) and (10^{-2} M) of other anions in THF (absorbance recorded at 390 nm).

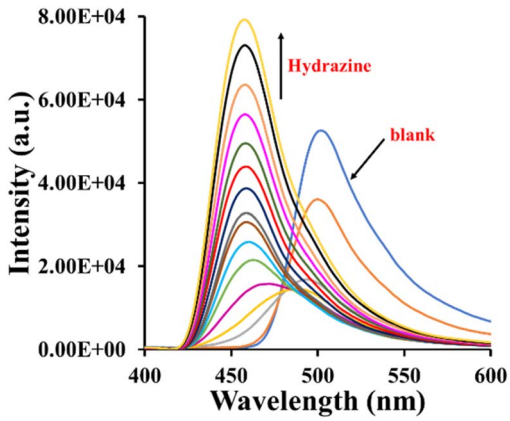

Fig. 3 Overlaid emission spectra of probe 1 (10^{-3} M) with hydrazine (10^{-3} M) in THF.

dicyanovinyl moiety. On adding hydrazine solution (10^{-3} M in THF), the intensity of the peak at 504 nm decreases with the appearance of a new peak at 460 nm. Upon titrating further, the peak at 504 nm disappears completely with an increase in the intensity of the new peak at 460 nm (Fig. 3). These ratiometric changes in the emission spectra again indicate the formation of a new compound between the probe and hydrazine. As the hydrazine molecule displaces the dicyanovinyl group, forming an imine bond, the ICT transition is inhibited completely, giving rise to ratiometric changes.

In the emission spectra, it was noticed that the changes were slightly less significant with lower concentrations of the probe and hydrazine. Owing to this, 10^{-3} M concentration of both the probe and hydrazine is used for the fluorescence titration experiment.

3.6. Sensing study of cyanide by the probe

The literature studies suggest that malononitrile-based sensors are sensitive towards cyanide ions. Similar experiments were also carried out for cyanide ions. As expected, with the addition of a TBACN solution, the absorbance at 428 nm decreases, and

a new peak at 386 nm appears with an isosbestic point at 389 nm (Fig. S6†). In the process, the colour of the solution changed from yellow to colourless, which enabled naked-eye detection of CN^- ion. This may be attributed to the disruption of the conjugation of the malononitrile moiety with anthracene moiety when adding CN^-. An isosbestic point at 389 nm indicates a one-to-one interaction between the probe and the ion.

Based on the changes in absorption, the binding constant of the interaction between the cyanide ion and the probe was calculated using the Benesi–Hildebrand equation and found to be $9.236 \times 10^3\ M^{-1}$ (Fig. S7a†), and the detection limit was found to be 0.16 μM (Fig. S7b†), which is much below the permissible limit of cyanide recommended by the World Health Organization (WHO) (2 μM).[37] Moreover, compared with many previously reported probes, the detection limit for CN^- ion was found to be impressive as it was superior (Table S2†).

Comparatively, the absorption spectra of the probe in the presence of hydrazine and CN^- were found to be significantly different, indicating different modes of interactions of the probe with these analytes. In the case of hydrazine, ratiometric changes were observed, suggesting the formation of a new compound with the addition of hydrazine. However, for CN^-, no such changes occurred, indicating the formation of an addition product rather than a completely new compound. Also, the colour changes in both cases justify the changes in their respective absorption spectra. Thus, in this way, both the analytes can be distinguished from one another, which also eliminates the chances of interference between the two.

Again, the literature suggests that chemodosimeters for cyanide ion are sensitive towards the S^{2-} ion, therefore a similar titration experiment was carried out for the mentioned ion using 10^{-3} M of S^{2-} in THF : H_2O and 10^{-4} M probe solution in THF : H_2O. In the case of S^{2-}, the THF : H_2O mixed solvent is used as a sensing medium since Na_2S is not completely soluble in THF. Although similar changes in absorption were observed by adding S^{2-}, the sensitivity of the probe towards S^{2-} was significantly less compared to the cyanide ion (Fig. S8†). It is worth noting that S^{2-} detection cannot be extended to lower concentration levels as the probe is very poorly sensitive towards it. When the probe concentration is lowered below 10^{-5} M, it cannot detect the presence of S^{2-}. In such cases, the probe can detect S^{2-} only if it is present in very high concentrations. The observed difference in sensitivity between these ions may be due to their difference in nucleophilicity. The CN^- ion possessing higher nucleophilicity can easily react with the C=C double bond of the dicyanovinyl moiety unlike S^{2-}. The sensitivity of the probe towards the nucleophilicity of the ions enables the selective detection of CN^- over S^{2-} unlike the chemodosimeters reported so far.

The sensing experiments were also performed for the probe with the above-mentioned ions namely F^-, Cl^-, Br^-, I^-, CN^-, AcO^-, N_3^- and SCN^-, in THF. No changes were observed in the absorption spectra of the probe for these ions (Fig. S9†).

3.7. Selective sensing of CN^- in the presence of S^{2-} ion

Since the probe can detect both CN^- and S^{2-}, it is necessary that it can selectively detect CN^- when both the ions are present. For the selective sensing of CN^- in the presence of S^{2-}, a separate experiment was performed in the presence of both ions. To a solution containing both the ions in THF : H_2O, a probe solution in THF : H2O was added. After that, a solution of $Pb(OAc)_2$ was added to the mixture. The solution turns brown immediately and a black precipitate is obtained due to the formation of PbS. The precipitate is then allowed to settle down. This is further centrifuged to remove the resulting PbS precipitate, and the supernatant liquid is collected (Fig. 4). The UV-vis spectra of this solution were also recorded, which shows that the probe can selectively detect CN^- in the presence of S^{2-} (Fig. S10†). This experiment confirms that in the presence of both ions, the probe selectively detects CN^- and the S^{2-} ions remain unreacted.

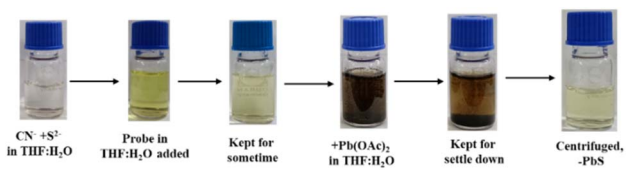

Fig. 4 Experiment performed for selective sensing of CN^- in the presence of both S^{2-} and CN^-. $Pb(OAc)_2$ was added to the mixture after the addition of the probe to remove S^{2-} as PbS.

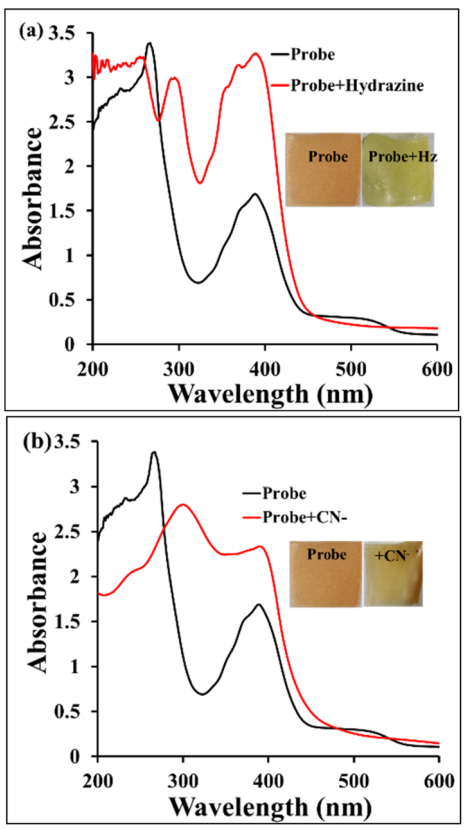

Fig. 5 Solid state absorption spectra of the probe@starch-PVA matrix before and after treatment with (a) hydrazine and (b) CN^- solution.

3.8. Solid state sensing

After the successful and sensitive detection of hydrazine and CN^- in solution by the probe in the solution phase, the sensing experiment is extended to the solid state of the probe for on-site detection of the analytes. For this, the probe is immobilized in the starch-PVA matrix. The preparation of probe@starch-PVA is given in S1.† The immobilized probe is obtained as a thin film, which is further used for the sensing purpose. To check the sensing properties, a strip of the film is dipped in hydrazine and CN^- ion solutions separately and dried. The colour of the strip changes from orange to light green in the case of hydrazine, whereas in the case of CN^-, the colour changes to colourless. The solid-state absorption spectra were recorded for both the changes. From the spectra, it was found that on the addition of hydrazine, a new peak appeared at 297 nm and the peak at 268 nm shifted to 260 nm (Fig. 5a). In the case of CN^-, a new peak appears at 302 nm and the peak at 268 nm disappears (Fig. 5b). These visual as well as spectral changes signify that our probe can detect hydrazine and CN and distinguish the two. Thus, the present probe has significant potential to be an on-site sensor for the detection of both hydrazine and CN^-.

Again, paper strip experiments were performed for the probe. Only for hydrazine (Fig. 6a and b) and CN^- ion (Fig. S11a and b†), the changes in colour of the strips were witnessed and for other analytes, strips remained unchanged.

In addition to the above experiments, sensing of both hydrazine and CN^- ion was done using the probe while adsorbed onto the silica surface. For this, 2 mL of 1 mM solution of the probe was mixed with 2 g of silica gel (60–120 mesh) and the solvent was evaporated to get a yellow crystalline silica powder (silica adsorbed with the probe). This was then treated with a hydrazine/CN^- ion solution (1 mM) in THF (2 mL) and dried in an oven at 50 °C. In the case of hydrazine, the changes in the colour of probe@silica from yellow to light green can be detected by the naked eye (Fig. 6c). While in the case of CN^-, the colour changes to colourless (Fig. S11c†).

Thus, all these experiments suggest that the probe has the potential to be used as a solid sensor.

3.9. Vapor phase sensing of hydrazine

Since hydrazine is volatile, the vapor phase sensing of hydrazine is also conducted. The TLC plates were taken in rectangular strips and soaked in the THF solution of the probe (10^{-5} M). The strips were then suspended over hydrazine solution in a closed chamber at room temperature. When observed after a few minutes (approximately 2–3 minutes), the colour of the strips changed from their original colour to light green, as observed in the case of solution and solid-state sensing experiments. Two hydrazine solutions were used for this experiment, *viz.*, 10^{-4} M and 10^{-2} M. The change in colour of the strips was found to be directly proportional to the concentration of hydrazine. Although the changes were very rapid for both, the colour transition was comparatively faster for a 10^{-2} M hydrazine solution (Fig. 7) than in the case of 10^{-4} M (Fig. S12†) solution. Thus, our probe is applicable for the detection of hydrazine in all three phases, *i.e.*, solid, liquid and vapor.

Fig. 7 Colour changes of the probe in the vapor phase upon exposure to 10 mM hydrazine solution.

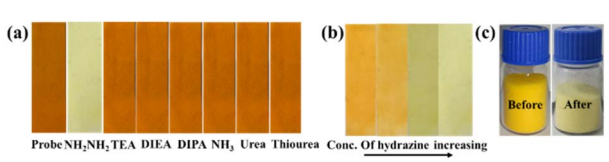

Fig. 6 (a) Test strips of probe 1 with different amines, (b) colour changes with increasing concentration of hydrazine, and (c) colour changes of probe 1 in the solid state upon the addition of hydrazine solution in THF.

3.10. Application of the probe in real sample analysis

To extend the applicability of the probe in real life, sensing of some real-life samples was performed. Water samples and soil samples were chosen for the detection of hydrazine and cyanide; water and some food extracts (Apple seeds and sprouted potato) were chosen for the experiment.

For the water sample analysis, we took different tap water samples. However, these water samples were devoid of hydrazine and cyanide. Hence, a known amount of hydrazine and CN^- ion was deliberately added to these samples by a standard addition method to perform the sensing experiment. The absorption spectra of the probe with water samples are shown in Fig. S13 and S15† for hydrazine and CN^-, respectively. The probe can detect hydrazine and CN^- ion with good recovery in these samples, as shown in Tables S3 and S4,† respectively. The calibration curves for both hydrazine and CN^- were found to have a good linear correlation between the absorbance and concentration with a correlation coefficient (R^2) value of 0.98 for hydrazine (from LOD curve) and 0.9888 for CN^-, (Fig. S14†), respectively.

For the detection of hydrazine in different soil samples, *viz.*, field soil, campus soil and garden soil were collected. The analytical procedures for the preparation of soil samples are given in S2.† The raw soil samples were tested with the probe for hydrazine content but were found to be devoid of it. So, they were pre-spiked with a known concentration of hydrazine solution and then tested again. The absorption spectra were recorded hereafter and our probe could successfully detect hydrazine in the soil samples with good recovery (Fig. 8 and Table S5†). Thus, our synthesized probe works well for the detection of hydrazine in real-world samples.

For the detection of cyanide content in food samples, apple seeds and sprouted potatoes were taken as these are known for

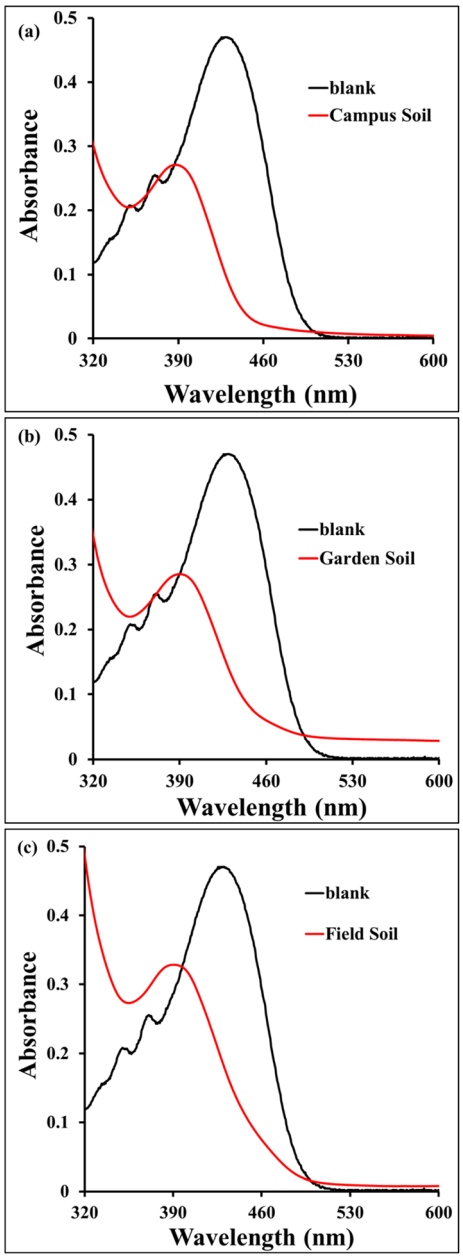

Fig. 8 Absorption spectra of the probe with soil samples for detection of hydrazine.

containing cyanide. The preparation of food samples is given in S3.†

The probe solution in THF : H_2O (10^{-4} M) was used to analyse the food extracts. Pronounced changes were observed in the absorption spectra of the probe in the presence of both extracts (Fig. S16a and b†). Thus, the probe was effective in the selective sensing of cyanide content in real-life samples. Moreover, the test strip experiment is extended to real samples, considering apple seed extract as a representative. The results are similar to those found for CN^- ions (Fig. S16c†). These attractive features make our probe appealing since it does not rely on sophisticated instrumentation and can be used for simple measurements.

3.11. Day-wise examination of potato extract samples

To investigate the change in the CN^- content in potato extracts with the extent of the sprouting of potatoes, we have carried out the experiment at different times. When the potato sample just began sprouting, it was considered as day 1 in the sensing analysis. Similarly, seven extracts were obtained from the sprouting of potato samples for 7 days. On day 7, the fully sprouted potato is taken for analysis. The UV-vis spectra of the samples were recorded (Fig. S17†), which shows that the absorbance of all the samples was almost equal. Since absorbance is directly related to the concentration of the substrate, when considering whether it is a partially or fully sprouted potato, they accumulate almost equal amounts of CN^-.

3.12. RGB analysis

The colour changes of the probe upon the addition of hydrazine and CN^- can also be evaluated in terms of the RGB content. Colorimetric sensors are well known as an economical and compact device in which light gets distributed into sets of colours, mainly red (R), green (G) and blue (B). Thus, the colour changes were evaluated by measuring the RGB content in the solutions using the computer application (ImageJ 1.53e, Java 1.8.0 _172). From the analysis, it was found that the RGB content in the probe solution before and after the addition of hydrazine and CN^- are different (Table 1 and Fig. S18†).

The 3D surface interactive plots for the probe@starch-PVA matrix were interpreted using the same application (Fig. S19†). The plots show different colour intensities for each solution, which indicates that the three plots represent different compounds.

3.13. Mechanism study

Although the mechanism is obvious from all the spectral data, the same ^1H and ^{13}C-NMR titration was done for the probe with hydrazine for confirmation. Also, the formation of a new compound of the probe with both hydrazine and cyanide was verified by recording the LC-MS spectra of the mixtures.

The NMR spectral changes produced by adding hydrazine to the probe were monitored at room temperature in a $CDCl_3$ solvent. On the addition of hydrazine, the peak at 8.67 ppm, corresponding to the vinylic proton shifts to 8.44 ppm, which is in agreement with the formation of the imine bond. Also, a new peak at 5.97 ppm arises, which is due to the amine protons of hydrazine (Fig. 9).

In the ^{13}C spectra, the vinylic carbon at 160.68 ppm shifted to 140.89 ppm, which corresponds to the imine carbon atom. Moreover, the carbon atoms of vinylic carbons disappeared by

Table 1 RGB content of the probe solution before and after the addition of hydrazine and CN^-

Sample	Red	Green	Blue
Host	202.24	188.292	24.1
Host + Hz	201.961	203.99	157.882
Host + CN^-	160.027	156.757	148.071

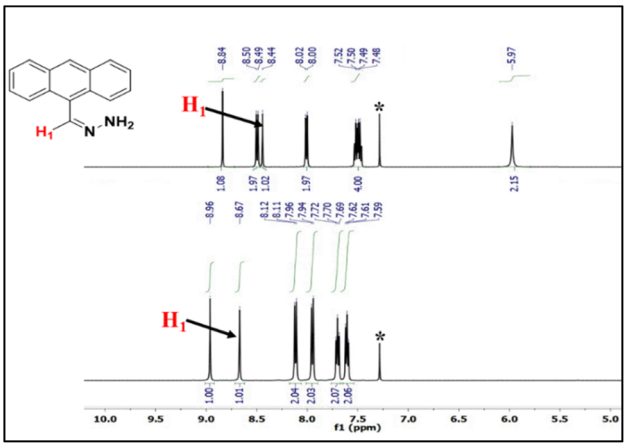

Fig. 9 ^{1}H-NMR spectral changes of the probe with and without hydrazine in $CDCl_3$.

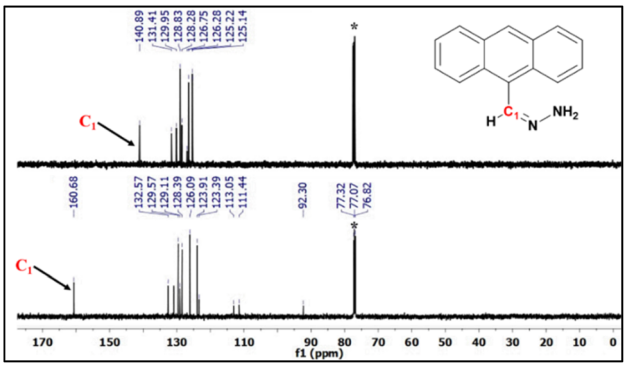

Fig. 10 ^{13}C-NMR spectral changes of the probe with and without hydrazine in $CDCl_3$.

adding hydrazine (Fig. 10). This further validates the formation of a new imine compound between the probe and hydrazine.

The LC-MS spectra of the probe with hydrazine show a peak at $m/z = 221.17$. This corresponds to the $[M + 1]^+$ peak of the desired imine product (Fig. S18†). Thus, all this information gathered is sufficient to confirm the plausible mechanism of the reaction between the probe and hydrazine.

Similar titrations were done in the case of CN^- although the reaction is pronounced as a nucleophilic addition of CN^- to the C=C bond. The mechanism is monitored by spectral changes produced by the addition of CN^- (as TBACN) to the probe in $CDCl_3$ at room temperature. In the ^{1}H-NMR spectra, the vinylic proton at δ 8.66 ppm completely disappears on the addition of CN^- and a new peak arises at 5.76 ppm (Fig. S19†). In addition, the aromatic protons also show a significant upfield shift that clearly indicates the disruption of the conjugation between the anthracene moiety and the dicyanovinyl moiety.

The mechanism is further explained by a ^{13}C-NMR titration. On the addition of CN^-, a new peak at δ 122.2 ppm arises, which corresponds to the new CN^- added to the C=C double bond. In addition, the peak at δ 160.68 ppm corresponding to C_1 of the dicyanovinyl group is shifted to δ 30.71 ppm and the peak at δ 92.30 ppm (C_2) is shifted to δ 18.10 ppm (Fig. S20†). These significant upfield shifts of the ^{13}C-NMR peaks represent the breaking of the C=C double bond. These observations are sufficient to confirm the mechanism as the nucleophilic addition of CN^- to the C=C bond.

The formation of a new addition compound was again confirmed from the LC-MS spectra (Fig. S21†).

3.14. Theoretical study

The ground state optimized geometries for the probe before and after the reaction with hydrazine represented as the reactant and the product, respectively, are shown in Fig. S22.† The atoms are labeled and numbered for clarity. The dihedral angle between the C9–C10–C15 and C10–C15–C16 planes in the reactant is −49.07° while the same dihedral angle for the product becomes −44.16°.

3.14.1 UV-vis spectra. The UV-vis spectra obtained from the STEOM-CCSD method employing the DLPNO scheme for the present probe suggest a peak at 436 nm (see Fig. 11a). The S_0 to S_1 transition includes the HOMO to LUMO, HOMO to LUMO + 1, and HOMO − 3 to LUMO + 1 transitions. The majority contribution of 87.2% comes from the HOMO to LUMO transition. The electron density plots of all four molecular orbitals involved in this transition are shown in Fig. 11b. The electron density maps suggest that in the case of HOMO, the electron is mostly located in the anthracene moiety, while in the case of LUMO and LUMO + 1, the density is distributed over the whole molecule.

In the case of the product, *i.e.*, the probe, after the reaction with hydrazine, the 436 nm peak disappeared (Fig. 12a). The S_0 to S_1 transition is observed at 360 nm; however, as suggested by

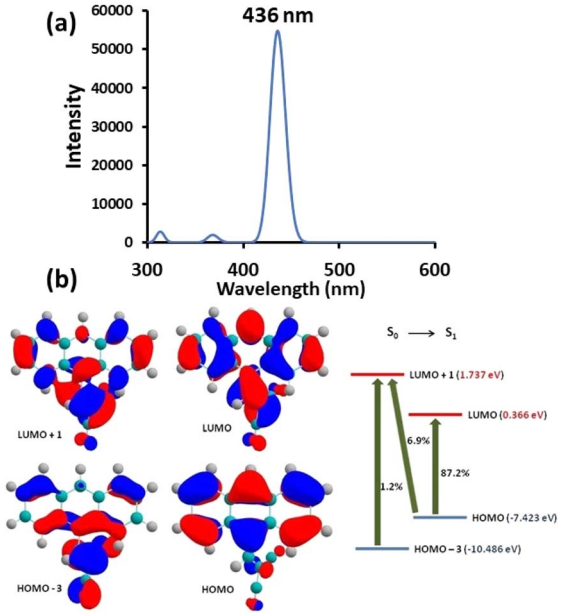

Fig. 11 (a) Simulated absorption spectra and (b) surfaces of the molecular orbitals involved in transitions, and their electron density plot of probe 1 (reactant).

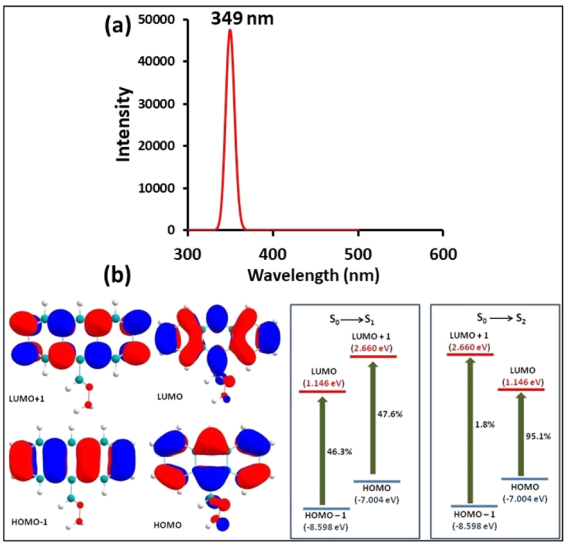

Fig. 12 (a) Simulated absorption spectra and (b) surfaces of the molecular orbitals involved in transitions, and their electron density plot of probe 1 after reaction with hydrazine (product).

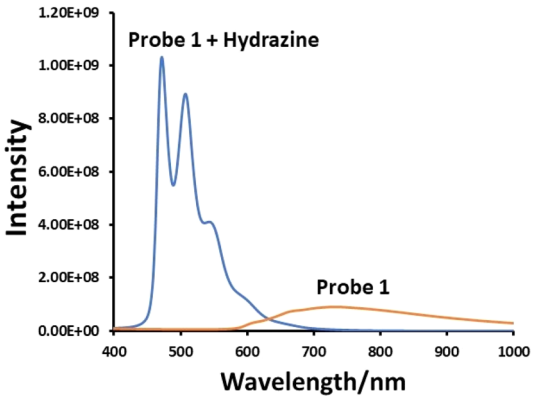

Fig. 13 TD-DFT predicted fluorescence spectra of probe 1 before and after reaction with hydrazine.

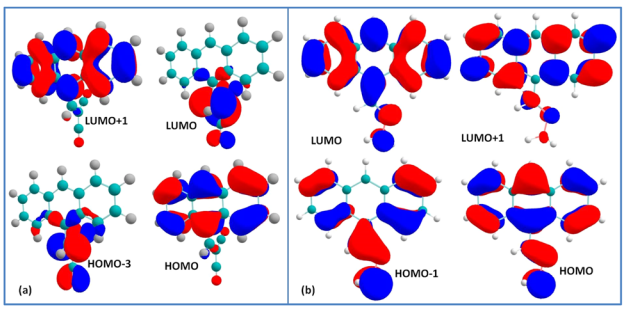

Fig. 14 Surfaces of molecular orbitals associated with excitation of the probe 1 (a) before and (b) after the addition of hydrazine.

a very low transition electric dipole moment, this transition could be a forbidden transition. The S_0 to S_1 transition includes a 46.3% contribution from HOMO − 1 to LUMO while a 47.6% contribution from the HOMO to LUMO + 1 transitions. The S_0 to S_2 transition is observed at 349 nm. This transition consists of a 1.8% contribution from HOMO − 1 to LUMO + 1 and a 95.1% contribution from HOMO to LUMO transition (Fig. 12b). It is important to note that for all the four molecular orbitals, *i.e.*, HOMO − 1, HOMO, LUMO and LUMO + 1, the electron density is mostly located at the anthracene moiety.

The details of the UV-vis spectra of both reactant and product are given in Table S6.†

3.14.2 TD-DFT with excited state optimization for fluorescence spectra. The TD-DFT optimized excited state (S1) geometries of both reactant and product are shown in Fig. S23.† The change in product geometry upon excitation is much less than the reactant geometry. In the case of the reactant, the dihedral angle between the anthracene and malononitrile planes changes from −49.07° to −89.97°. The planes are nearly perfectly perpendicular to each other upon excitation. In the case of the product, a slight decrease in the dihedral angle (from −44.16° to −14.49°) is observed. These observations have important implications for the predicted fluorescence spectra of both reactant and product. As depicted in Fig. 13, in the case of the reactant, the fluorescence (red solid line) intensity is negligible compared to the product and the peak is observed at 731 nm while strong fluorescence peaks are observed for the product at 472 nm, 507 nm, and 543 nm. The excited state electron density maps are plotted in Fig. 14a and b for the reactant and product, respectively.

Fig. 14a shows that in the case of the reactant, the LUMO is localized in the malononitrile moiety while HOMO is localized in the anthracene moiety. Therefore, the LUMO to HOMO transition could have been the major contributor to fluorescence; however, the ICT is difficult because the planes are now perpendicular to each other, and hence, fluorescence is not observed in the case of the reactant.

From the above discussion, it is obvious that the theoretical findings comply with the experimental results obtained. Also, the theoretical calculation gives insight into the possibility of an intramolecular charge transfer in the probe before and after reacting with hydrazine. Thus, the theoretical study can also be a tool to examine the sensing mechanism of the probe.

4. Conclusion

To sum up, we have designed and synthesized an easy-to-make probe for selective sensing of hydrazine and CN^- through colorimetric and fluorometric methods. The probe can detect both analytes with a very low detection limit of 1.7 ppb and 4.16 ppb. It works through a chemodosimetric approach by cleavage of the dicyanovinyl moiety through hydrazine while in the case of CN^-, the nucleophilic addition of CN^- to the C=C double bond occurs. The probe can also be used as a solid or paper-based sensor for the on-site detection of both analytes. To extend the same, it is immobilized in a starch-PVA film, which also shows pronounced changes both visually and spectrophotometrically. Moreover, the application of the probe is successfully extended to real samples. Furthermore, the mechanism of sensing was confirmed by NMR titration as well as

mass spectra. Thus, all these thorough experimental data support the fact that probe 1 can serve as a highly selective and sensitive chemosensor for both hydrazine and CN^- ion.

Data availability

The data supporting this article have been included as part of the ESI.†

Author contributions

Jhorna Borah: conceptualization, investigation, methodology, resources, data curation, visualization, writing – original draft. Arati Chetry: investigation, methodology, resources, data curation. Anisha Pegu: investigation, methodology, resources, data curation. Pankaj Dutta: fluorescence measurement, supervision. Anupaul Baruah: investigation, methodology, software. Prithiviraj Khakhlary: conceptualization, investigation, methodology, resources, visualization, writing-review & editing, supervision.

Conflicts of interest

There are no conflicts to declare.

Acknowledgements

The authors thank the Science and Engineering Research Board, Govt. of India (EEQ/2019/000139) and Department of Science and Technology, Govt. of India (SR/PURSE/2022/142(C)) for funding this work. The authors also thank the CIF, Dibrugarh University, for instrumental support.

Notes and references

1 F. Amiripour, S. N. Azizi and S. Ghasemi, *Biosens. Bioelectron.*, 2018, **107**, 111–117.
2 J. Qiu, Y. Chen, S. Jiang, H. Guo and F. Yang, *Analyst*, 2018, **143**, 4298–4305.
3 A. A. Bhosle, M. Banerjee, S. Saha, S. Garg, S. Ghosh and A. Chatterjee, *Sens. Actuators, B*, 2023, **397**, 134661.
4 M. Z. Dai, Y. Lo Lin, H. C. Lin, H. W. Zan, K. T. Chang, H. F. Meng, J. W. Liao, M. J. Tsai and H. Cheng, *Anal. Chem.*, 2013, **85**, 3110–3117.
5 C. A. S. Pothulapadu, A. Jayaraj, N. Swathi, R. N. Priyanka and G. Sivaraman, *ACS Omega*, 2021, **6**, 24473–24483.
6 S. Tšupova, O. Lebedev and U. Mäeorg, *Tetrahedron*, 2012, **68**, 1011–1016.
7 K. Tiensomjitr, R. Noorat, S. Chomngama, K. Wechakorn, S. Prabpai, P. Kanjanasirirat, Y. Pewkliang, S. Borwornpinyo and P. Kongsaeree, *Spectrochim. Acta, Part A*, 2018, **195**, 136–141.
8 K. F. Khaled, *Appl. Surf. Sci.*, 2006, **252**, 4120–4128.
9 V. Rosca and M. T. M. Koper, *Electrochim. Acta*, 2008, **53**, 5199–5205.
10 X. Yanga, Y. Liua, Y. Wub, X. Renb, D. Zhangc and Y. Ye, *Sens. Actuators, B*, 2017, **253**, 488–494.
11 Q. Yi, J. He, X. Fu, J. Ying, L. Gong, J. Shen and X. He, *Dyes Pigm.*, 2021, **196**, 109816.
12 J. Kou, Z. Meng, X. Wang, Z. Wang and Y. Yang, *React. Funct. Polym.*, 2023, **182**, 105453.
13 J. Sanabria-Chinchilla, K. Asazawa, T. Sakamoto, K. Yamada, H. Tanaka and P. Strasser, *J. Am. Chem. Soc.*, 2011, **133**, 5425–5431.
14 B. Roy, S. Halder, A. Guha and S. Bandyopadhyay, *Anal. Chem.*, 2017, **89**(19), 10625–10636.
15 X.-X. Zhao, J.-F. Zhang, W. Liu, S. Zhou, Z.-Q. Zhou, Y.-H. Xiao, G. Xi, J.-Y. Miao and B.-X. Zhao, *J. Mater. Chem. B*, 2014, **2**, 7344.
16 U. N. Guria, S. K. Manna, K. Maiti, S. K. Samanta, A. Ghosh, P. Datta, D. Mandale and A. K. Mahapatra, *New J. Chem.*, 2021, **45**, 15869–15875.
17 S. Goswami, A. K. Das, U. Saha, S. Maity, K. Khanra and N. Bhattacharyya, *Org. Biomol. Chem.*, 2015, **13**, 2134–2139.
18 S. K. Manna, A. Gangopadhyay, K. Maiti, S. Mondal and A. K. Mahapatra, *ChemistrySelect*, 2019, **4**, 7219–7245.
19 B. Lv, Z. Wang, Y. Wu, Y. Zheng, Z. Cui, J. Li and W. Gu, *J. Hazard. Mater.*, 2024, **469**, 134105.
20 J. Zhang, W. Gao, M. Dou, F. Wang, J. Liu, Z. Li and J. Ji, *Analyst*, 2015, **140**, 1686–1692.
21 S. Virji, R. B. Kaner and B. H. Weiller, *Chem. Mater.*, 2005, **17**, 1256–1260.
22 R. D. Crapnell and C. E. Banks, *Sens. Diagn.*, 2022, **1**, 71–86.
23 B. Roy, S. Halder, A. Guha and S. Bandyopadhyay, *Anal. Chem.*, 2017, **89**(19), 10625–10636.
24 S. Feng, H. Yu, X. Zhang, L. Huo, R. Gao, P. Wang, X. Cheng, Z. Major, S. Gao and Y. Xu, *Sens. Actuators, B*, 2022, **359**, 131529.
25 G. Lu, S. Yu, L. Duan, S. Meng, S. Ding and T. Dong, *Spectrochim. Acta, Part A*, 2024, **305**, 123450.
26 K. Rajalakshmi, S. Muthusamy, H.-J. Lee, P. Kannan, D. Zhu, R. S. Lodi, M. Xie, J. Xie, J.-W. Song and Y. Xu, *Spectrochim. Acta, Part A*, 2024, **304**, 123282.
27 M. J. Jung, S. J. Kim and M. H. Lee, *ACS Omega*, 2020, **5**, 28369–28374.
28 W. Xu, X. Li, J. Yin, M. Han, W. Liu, Y. Yang and W. Li, *J. Photochem. Photobiol., A*, 2020, **390**, 112262.
29 S. Zhang, D. Chen, L. Yan, Y. Xie, X. Mu and J. Zhu, *Microchem. J.*, 2020, **157**, 105066.
30 Y. Chen, W. Mo, Z. Cheng, F. Kong, C. Chen, X. Li and H. Ma, *Dyes Pigm.*, 2022, **198**, 110004.
31 S. I. Reja, N. Gupta, V. Bhalla, D. Kaur, S. Arora and M. Kumar, *Sens. Actuators, B*, 2016, **222**, 923–929.
32 A. D. S. Schramm, R. Menger and V. G. Machado, *J. Mol. Liq.*, 2016, **223**, 811–818.
33 E. V. Anslyn, *J. Org. Chem.*, 2007, **72**, 687–699.
34 Z. Guo, T. Hu, T. Sun, T. Li, H. Chi and Q. Niu, *Dyes Pigm.*, 2019, **163**, 667–674.
35 A. Kakoti, R. Rohman, R. Kar and P. Khakhlary, *ChemistrySelect*, 2022, **7**, e202202412.
36 G.-J. Kim and H.-J. Kim, *Tetrahedron Lett.*, 2010, **51**, 2914–2916.
37 J. Hwang, T. S. Reddy, H. Moon, H. D. Lee and M.-S. Choi, *Dyes Pigm.*, 2023, **215**, 111243.

38 N. Kumari, S. Jha and S. Bhattacharya, *J. Org. Chem.*, 2011, **76**, 8215–8222.
39 Q. Li, Y. Cai, H. Yao, Q. Lin, Y.-R. Zhu, H. Li, Y.-M. Zhang and T.-B. Wei, *Spectrochim. Acta, Part A*, 2015, **136**, 1047–1051.
40 R. Bhaskar and S. Sarveswari, *Inorg. Chem. Commun.*, 2019, **102**, 83–89.
41 L. Long, X. Yuan, S. Cao, Y. Han, W. Liu, Q. Chen, Z. Han and K. Wang, *ACS Omega*, 2019, **4**, 10784–10790.
42 J. Borah, U. N. Hazarika and P. Khakhlary, *ACS Omega*, 2022, **7**, 46234–46240.
43 S. Park and H.-J. Kim, *Chem. Commun.*, 2010, **46**, 9197–9199.
44 R. Jackson, R. P. Oda, R. K. Bhandari, S. B. Mahon, M. Brenner, G. A. Rockwood and B. A. Logue, *Anal. Chem.*, 2014, **86**(3), 1845–1852.
45 A. Dvivedi, P. Rajakannu and M. Ravikanth, *Dalton Trans.*, 2015, **44**, 4054–4062.
46 M. D Hanwell, D. E Curtis, D. C Lonie, T. Vandermeersch, E. Zurek and G. R Hutchison, *J. Cheminf.*, 2012, **4**, 1–17.
47 F. Neese, F. Wennmohs, U. Becker and C. Riplinger, *J. Chem. Phys.*, 2020, **152**, 224108.
48 Graphical software for visualization of quantum chemistry computations, Version 1.8, build 654, **https://www.chemcraftprog.com**.